nanomanufacturing

MDPI

Article

Solvent-Mediated Structural Evolution Mechanism from Cs_4PbBr_6 to $CsPbBr_3$ Crystals

Felipe A. La Porta [1,2,*] and Sofia Masi [2]

[1] Laboratory of Nanotechnology and Computational Chemistry (NanoQC), Federal Technological University of Paraná (UTFPR), Londrina 86036-370, PR, Brazil
[2] Institute of Advanced Materials (INAM), Universitat Jaume I, Av. Sos Baynat, s/n, 12006 Castelló, Spain; masi@uji.es
* Correspondence: felipelaporta@utfpr.edu.br

Abstract: The study of the solvent-mediated structural evolution mechanism of the Cs_4PbBr_6 powders prepared using the solvothermal method is presented. The Cs_4PbBr_6 powders with a rhombohedral structure and an intense green emission (i.e., mainly due to the presence of complex defect states in the forbidden gap), which is stable in its solid-state form, but a distinct behavior is observed in different dispersions, easily detectable when irradiated with ultraviolet (UV) light. Depending on the polarity of the solvent, a change in the emission color from green to red is observed, easily detectable when irradiated with ultraviolet (UV) light. Our findings suggest that the solvent polarity affects the surface decomposition process, leading to a different change in composition, structure and crystal shape. This peculiar behavior plays a pivotal role in the control of the properties of Cs_4PbBr_6, and this study, therefore, offers a fundamental understanding needed for Cs_4PbBr_6 potential future applications.

Keywords: solvothermal processing; Cs_4PbBr_6; perovskite; structural evolution; solvent effects

Citation: La Porta, F.A.; Masi, S. Solvent-Mediated Structural Evolution Mechanism from Cs_4PbBr_6 to $CsPbBr_3$ Crystals. *Nanomanufacturing* **2021**, *1*, 67–74. https://doi.org/10.3390/nanomanufacturing1020007

Academic Editors: Andres Castellanos-Gomez and Sotirios Baskoutas

Received: 10 April 2021
Accepted: 26 May 2021
Published: 5 July 2021

1. Introduction

All-inorganic, cesium lead, bromide-related compounds are promising for optoelectronic and photovoltaic applications and have therefore received considerable attention over the last decade [1–6]. Such compounds with a perovskite structure may exist in different stoichiometries such as $CsPbBr_3$, Cs_4PbBr_6 and $CsPb_2Br_5$, which are usually characterized by a difference in the stacking of $[PbX_6]^{4-}$ octahedra in the crystalline structure [1–4]. As is well-known, each crystalline structure has distinct physical and chemical properties. For instance, the bulk $CsPbBr_3$ and Cs_4PbBr_6 crystals have a direct bandgap (2.43 eV and 3.95 eV at room temperature, respectively) [4], with a low exciton binding energy of ~19–62 meV for $CsPbBr_3$ [7–9] and a large exciton binding energy of approximately 353 meV for Cs_4PbBr_6 [9]. Both structures are of significant interest in optoelectronic and photovoltaic applications compared to the bulk $CsPb_2Br_5$ phase, which exhibits an indirect bandgap of approximately 3.85 eV [10,11]. In this context, many researchers have studied various techniques for the fabrication of both $CsPbBr_3$ and Cs_4PbBr_6 materials, using numerous processing methods, although the crystal structure and the correlated properties are still unclear and debated in the literature [1–18]. Moreover, a significant limitation in the development of these materials is related to the large-scale fabrication, as currently, most of the available protocols to obtain Cs_4PbBr_6 crystals are based on the use of high purity reagents [19–21]. Consequently, it is necessary to develop new processing methods to facilitate the fabrication of large-scale, single-crystalline Cs_4PbBr_6-related compounds at a low cost, attractive to boost the emergence of new technologies, which in turn are not yet in the market due to the high cost of the final product.

Herein, we presented a solvothermal approach and a detailed study of structural, morphological and optical properties of Cs_4PbBr_6 crystals, in addition to their solvent-mediated structural evolution process. We observed that the Cs_4PbBr_6 crystals in solution

exhibit a distinct change of the emitted color, depending on the type of solvent used (dimethyl sulfoxide, DMSO, *N*,*N*-dimethylformamide, DMF and methyl acetate, MeOAc). To investigate the effects of the solvent-mediated structural evolution of the Cs_4PbBr_6 materials, we used field-emission scanning electron microscopy (SEM), in addition to ultraviolet-visible (UV-vis) and photoluminescence (PL) spectroscopy, in conjunction with electrochemical measurements. This study provides a new route for Cs_4PbBr_6 synthesis and an insight into the effects of solvent-mediated structural evolution in the photophysics responses of Cs_4PbBr_6 microcrystals as prepared.

2. Experimental

Cs_4PbBr_6 microcrystals were successfully synthesized based on the solvothermal method using approximately 5 mL of a solution of 6 M hydrobromic acid (HBr, 48%), together with 3.5 mmol of lead acetate trihydrate (Sigma-Aldrich, 99%, St. Louis, MO, USA) and 3.5 mmol of cesium carbonate (Sigma-Aldrich, 99%) in 10 mL of dimethyl sulfoxide into a Teflon autoclave at 150 °C for 120 min. Next, the resulting precipitate was then cooled to near room temperature and then immediately washed with acetone and ethanol several times in order to fully remove byproducts and dried at 80 °C overnight to obtain a green powder. A remarkable characteristic of this solvothermal approach is that it may, in principle, be scalable by an increase of the size of autoclave used [22]. The as-prepared powders were characterized using X-ray diffraction (XRD) in a 2θ range from 5° to 120° at 0.01° min^{-1}, using an X-ray diffractometer (D8 Advance, Bruker-AXS, Karlsruhe, Germany) with a Cu Kα source. Micro-Raman spectra are acquired using a Raman spectrometer model NRS-3100 (JASCO, Easton, MD, USA) using a 633 nm laser excitation source. The morphology and compositional analysis of the prepared Cs_4PbX_6 powders was analyzed using SEM (JEOL 7001F, Tokyo, Japan). In this case, the optical properties were then analyzed using UV-vis absorption spectroscopy with a Cary 300 Bio spectrophotometer (Agilent Technologies, Inc., Santa Clara, CA, USA) operating in the diffuse reflection mode. In this study, PL measurements, including their time-resolved PL spectra, were collected at room temperature using a Horiba-Fluorolog (Jobin Yvon, Longjumeau, France) for 350 nm excitation. The photoluminescence quantum yield (PLQY) was measured using an integrating sphere accessory with an excitation wavelength of 350 nm (Hamamatsu Photonics, Hamamatsu, Japan). For the study of the mechanism of structural evolution of these perovskites, different dispersions were prepared with concentrations of 10 $mg{\cdot}mL^{-1}$ Cs_4PbBr_6 crystals using dimethyl sulfoxide (DMSO), *N*,*N*-dimethylformamide (DMF) and methyl acetate (MeOAc) as the solvent. Next, for visualizing this specific process, the resulting dispersion was UV-irradiated for 120 min (UV bulb, 9 W, 365 nm). After 120 min there was no change significantly observed in our preliminary tests and, for this reason, we selected this time for our experiments. Thus, the kinetics of the solvent-mediated structural evolution of Cs_4PbBr_6 crystals were then monitored via SEM, UV-vis and PL measurements.

3. Results and Discussion

The pure Cs_4PbBr_6 has a typical structure with an ionic character higher than the one in the $CsPbBr_3$ structure, due to an increase of the Pb-Br bond length in Cs_4PbBr_6 [7,23]. In turn, this structure is considered much more tolerant of the incorporation of defects, compatible with many desired optoelectronic applications, especially in light-emitting devices or as battery components [23]. Consequently, this implies a stronger PL emission for Cs_4PbBr_6 crystals. However, the origin of this strong PL emission for the Cs_4PbBr_6 crystals is still debated [3,4,7,8]. These properties are supported by their crystalline structure, in which the clusters of ($PbBr_6$) are isolated and separated by ions of Cs [24]. As briefly mentioned above, the Cs_4PbBr_6 powder is synthesized for the first time from the solvothermal method and first characterized by the XRD measurements. Figure 1a illustrates the XRD patterns of Cs_4PbBr_6 powders that were processed under solvothermal conditions, where all the peaks can be correctly indexed to the rhombohedral phase with space group (ICSD # 162158). A high intensity of the (113) face for

the as-prepared Cs_4PbBr_6 crystals (compared to the ICSD # 162158) indicates a predominance of this exposed face (113) related to the solvothermal conditions used in this study. Figure 1b shows the crystallographic unit cell of the rhombohedral Cs_4PbBr_6 structure (belonging to space group R-3c (n° 167)) that is typically formed by octahedral (PbX_6) clusters separated by Cs ions [7,23,24]. The reaction at this temperature produces an assembly of cubic-like morphologies, which in turn leads to distinct shapes, as shown in the SEM images of the Cs_4PbBr_6 powders (Figure 1c). In addition, the EDS data (Figure 1d–g) confirms the presence of Cs, Pb and Br in agreement with the expected stoichiometry for the as-prepared Cs_4PbBr_6 crystals.

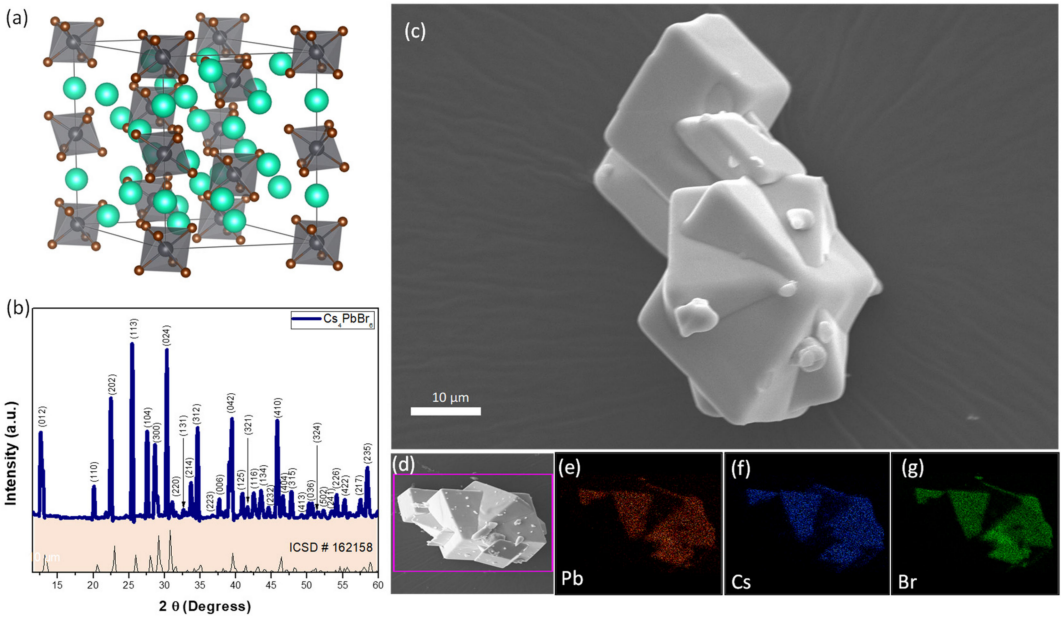

Figure 1. (**a**) Crystallographic unit cell, (**b**) XRD patterns, (**c**) SEM images and (**d**–**g**) EDX mapping of Cs_4PbBr_6 crystals.

The room-temperature micro-Raman spectra of single-crystalline Cs_4PbBr_6 (Figure 2A), display two Raman-active bands at approximately 80.64 cm^{-1} and 121.30 cm^{-1}, which are attributed to the vibration modes of the octahedral (PbX_6) clusters in the rhombohedral Cs_4PbBr_6 structure [7,25,26]. Additionally, the Raman intensity ($I_{80.64}/I_{121.30}$) ratio found for these crystals may be a possible indication that the halide vacancies are predominant in this structure. To investigate the optical response of the Cs_4PbBr_6 powders, the UV-vis and PL measurements are carried out. The Cs_4PbBr_6 materials exhibit an optical absorption spectrum that is governed by well-studied direct electronic transitions [7,27] and Figure 2B shows the UV-vis spectra of the Cs_4PbBr_6 powders with a peak absorption at approximately 520 nm. The calculated bandgap of the Cs_4PbBr_6 is ~3.59 eV (Figure 2B), according to the Kubelka–Munk method [28], a significantly lower value if compared with the literature (3.95 eV) [8]. The PL band in Figure 2D has a maximum emission at about 540 nm, in accordance with previous reports [3,7,9,29].

Notably, the PL emission spectra are then deconvoluted into three sub-peaks using the Gaussian function, as shown in Figure 2D, in which each of these components represents a different defect state within the forbidden bandgap [27]. The observed PL profile can be attributed to specific structural distortions in the octahedral (PbX_6) clusters [3,7,9,29,30]. Moreover, the PLQY measured for the Cs_4PbBr_6 powders is about 15%, indicating that the solvothermal method is an alternative way to synthesize a good-quality material on a large scale. As the lifetime constant (τ_1 = 19.63 ns) is usually associated with excitonic recombination, while τ_2 = 19.64 ms can be attributed to the different defect states that are generated during the synthesis of such samples [30]. However, the PLQY and decay time results for as-prepared pure Cs_4PbBr_6 microcrystals are in general lower and slower than reported in the literature [3,31]. However, it must be emphasized that different synthetic routes prepared the same materials used in this comparison. It is known that materials

processing is based on defect engineering. Thus, the final product will have more or fewer defects depending on the experimental conditions used in their manufacturing [32,33]. From this perspective, a similar material in terms of its physical characteristics (such as morphology, size, composition and structure) but prepared from the use of different synthetic routes exhibits completely different properties [32–34].

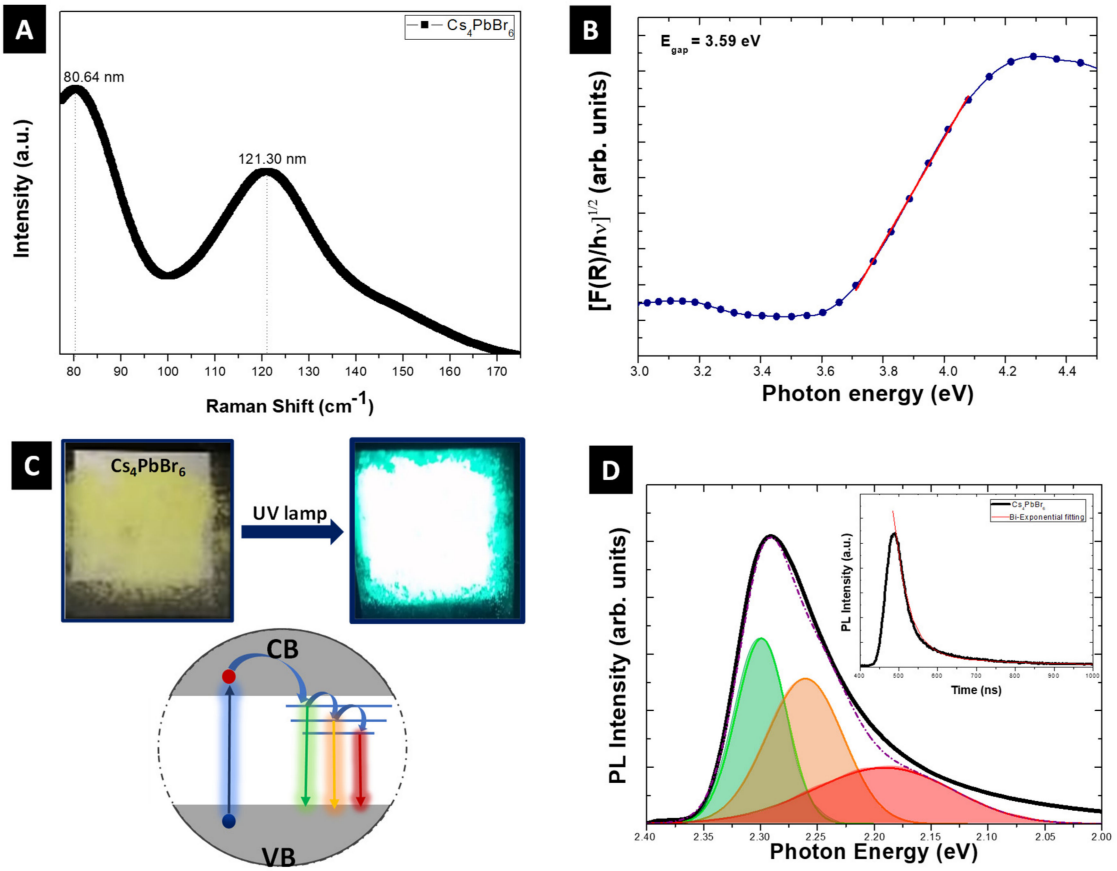

Figure 2. (**A**) Raman spectra, (**B**) UV-vis absorbance spectra (with inset of band gap calculated), (**C**) Digital photograph of the powder before and after irradiated by a UV lamp (below a schematic representation of the PL mechanism) (**D**) PL emission spectra and time-resolved PL decay spectra at 485 nm of the as-prepared Cs_4PbBr_6 crystals.

Considering its potential application in several emerging optoelectronic technologies, studies on its structural transformation and structural evolution process may reveal important chemical information regarding the stability of the material. As well-known, the as-prepared Cs_4PbBr_6 powders exhibit high intrinsic stability (e.g., both moisture and oxygen) [8]. Interestingly, we observed an unusual behavior of the as-prepared Cs_4PbBr_6 powders in solution (Figure 3A). Based on the polarity of the solvent used in this study (DMSO, DMF, MeOAc), a change in the color emitted (in solution) from green to red is observed. A detailed understanding of this unusual behavior is essential for the solution-processed devices, since this feature may ultimately affect the device performance. For a better understanding of the main steps of this structural evolution mechanism, we initially evaluated the photophysics properties of the three different dispersions, in DMSO, DMF and MeOAc, respectively, by means of UV-vis and PL measurements, which are compared in Figure 3B–E. Due to the low dispersibility of Cs_4PbBr_6 in MeOAc, it is hard to obtain reliable measurements, so only the comparison between the powder in DMSO and DMF is reported.

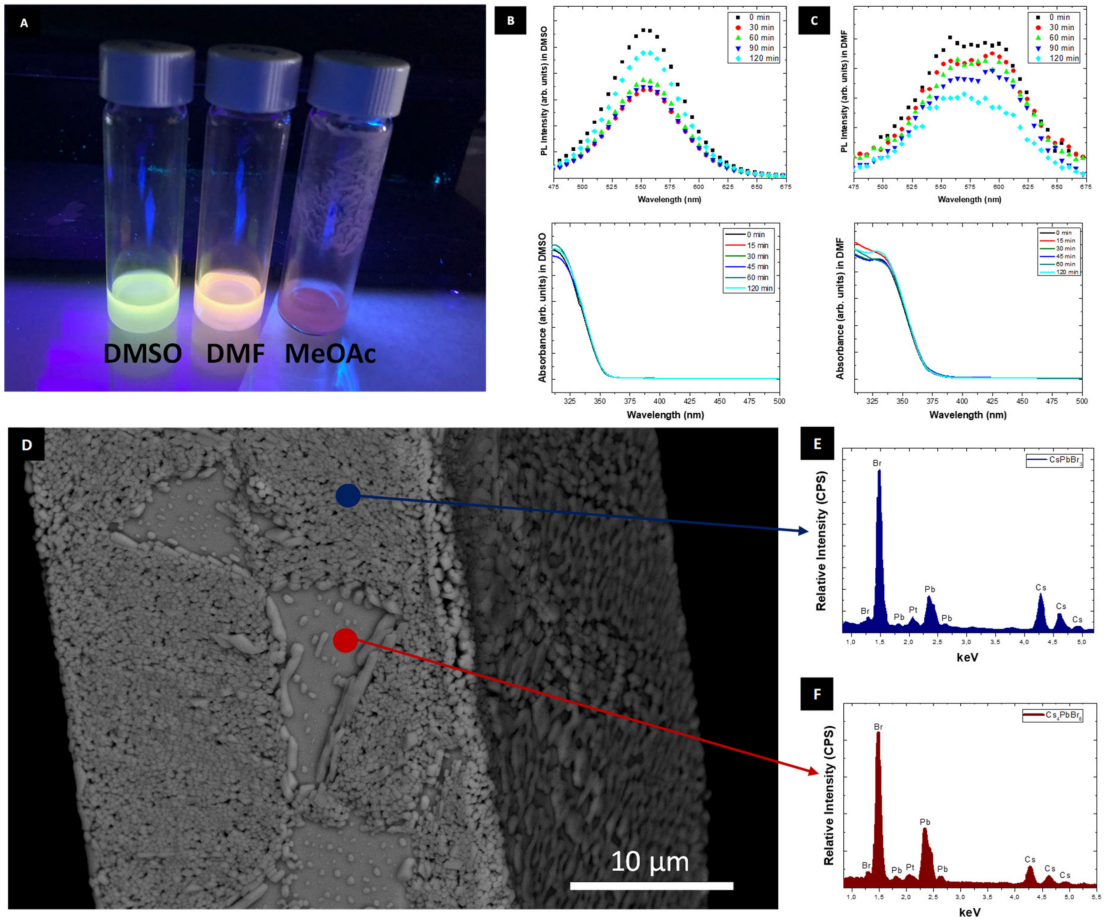

Figure 3. (**A**) Digital photos of the UV-irradiated dispersion of Cs_4PbBr_6 crystals at room temperature. UV-vis absorbance spectra and PL spectra at different times for the Cs_4PbBr_6 crystals in solution: (**B**) DMSO and (**C**) DMF. (**D**–**F**) Representative BSE-SEM with EDS analysis of the UV-irradiated dispersion of Cs_4PbBr_6 crystals after 120 min.

As expected, we observed a blue shift in the UV-vis absorbance spectra as a function of solvent polarity used in this experiment [35]. Therefore, we can observe that the change in solvent polarity alters their structural evolution kinetics behavior, suggesting that a lower polarity is responsible for a higher structural evolution rate for the Cs_4PbBr_6 crystals. In fact, the UV-vis absorption spectrum for all dispersions shows a small variation in time, being more meaningful for minor polarity solvent. These findings are in good agreement with PL measures, which show a smaller reduction of intensity PL for the Cs_4PbBr_6 in DMSO over time. In all cases, Cs_4PbBr_6 crystals in DMSO were the most optically stable dispersions. These photophysical results reveal a partial structural transformation of these samples. Our data thus suggest a possible stabilization of defect states by the solvent that likely also acts as a passivating agent.

From a structural point of view, these octahedral (PbX_6) clusters are isolated in the rhombohedral Cs_4PbBr_6 structure, which may indicate a weak interaction between them [7,23,24,27], and that the surface of these structures is highly flexible. Hence, we propose that the solvents can induce a partial structural evolution of the surface of the Cs_4PbBr_6 crystals, due to the interaction with the octahedral (PbX_6) clusters, in turn exchanging the CsBr and creating new surface states that modulate the emission of the solution. The extraction of CsBr is in fact already studied and leads to a phase transformation of Cs_4PbBr_6 into $CsPbBr_3$ [36–38], as we observed from the BSE-SEM images (Figure 3D) and EDS measurements in different regions after 120 min of solution aging. The chemical and morphological alteration of the crystals confirms that the solvent contributes to the decomposition of Cs_4PbBr_6 as we detect two different compositions (Cs_4PbBr_6 and $CsPbBr_3$) and also the

CsBr extracted residual outside the crystal (see Figure 4). The structural modifications in the solution are therefore the reason why the emission in the solution changes with the polarity of the solvent, which induces a partial chemical and structural transformation of the Cs_4PbBr_6 to $CsPbBr_3$, as well as a partial amorphization of the surface of these crystals.

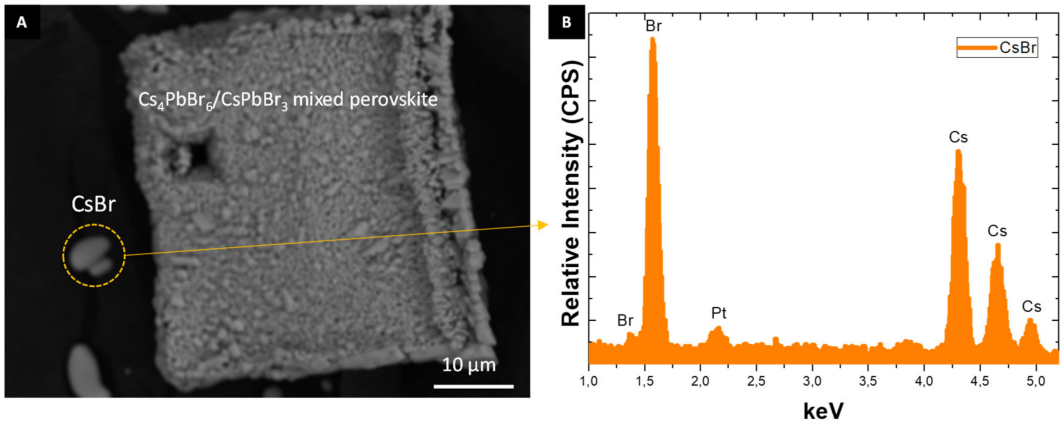

Figure 4. (**A**) BSE-SEM with (**B**) EDS analysis after partial structural evolution of Cs_4PbBr_6 crystals enables the detection of the CsBr species as a by-product.

In addition, the different suspensions of these crystals play a critical role in controlling the $CsPbBr_3$ final size. According to our SEM images (Figures 1 and 4), it seems that the structural evolution process is a sort of Kirkendall effect [39,40]. Furthermore, these results suggest that this process is not only limited to the surface of the material studied, but might in principle occur in the entire crystal, as well. Therefore, these kinetic data provide evidence of the critical role of the solvent in determining the properties of Cs_4PbBr_6. These results are consistent with the shift observed in the UV-vis and PL data. Also, it is worth highlighting that Cs_4PbBr_6 has a high dispersion in DMSO, which hence is the most suitable solvent for solution-based optoelectronic devices.

4. Conclusions

In summary, we reported the synthesis of the pure Cs_4PbBr_6 crystals by solvothermal method, with a rhombohedral structure, a green emission at normal room temperature (mainly due to the presence of complex defect states in the forbidden gap) and exhibiting a high PLQY. Moreover, we have demonstrated a solvent-mediated structural evolution process of the Cs_4PbBr_6 crystals to shine a light on the intrinsic stability of the as-prepared material. According to our findings, the chemical transformation of the surface of Cs_4PbBr_6 is promoted by the solvent, which can induce a color change for Cs_4PbBr_6 dispersions. This is related to the different extraction rates of the CsBr species (i.e., originating at the Cs_4PbBr_6 surface), which in turn depends on the polarity of the solvent used. With the increase of the solvent polarity, the structural evolution of the Cs_4PbBr_6 crystals is faster, resulting in a blue shift of the solution emission and a rearrangement of the structure and morphology following a Kirkendall-like mechanism. The modulation of phase composition $Cs_4PbBr_6/CsPbBr_3$ may therefore be beneficial for the performance of these devices, since the relative band position of these materials would, in theory, facilitate the recombination of holes and electrons. Furthermore, such effects could pave the way for the emergence of novel optoelectronic applications based on $Cs_4PbBr_6/CsPbBr_3$ materials.

Author Contributions: Conceptualization, F.A.L.P.; methodology, F.A.L.P.; software, F.A.L.P.; validation, F.A.L.P.; formal analysis, F.A.L.P. and S.M.; investigation, F.A.L.P. and S.M.; resources, F.A.L.P.; data curation, F.A.L.P. and S.M.; writing-original draft preparation, F.A.L.P. and S.M.; writing-review and editing, F.A.L.P. and S.M.; visualization, F.A.L.P. and S.M.; funding acquisition; F.A.L.P. All authors have read and agreed to the published version of the manuscript.

Funding: This work was supported by the Brazilian agencies Fundação Araucária, CAPES and CNPq (203012/2017-8).

Data Availability Statement: Not applicable.

Acknowledgments: F.A.L.P. is thankful to Iván Mora Seró, at University Jaume I, for their help with the support and discussion of these results.

Conflicts of Interest: The authors declare no conflict of interest.

References

1. Manser, J.S.; Christians, J.A.; Kamat, P.V. Intriguing Optoelectronic Properties of Metal Halide Perovskites. *Chem. Rev.* **2016**, *116*, 12956–13008. [CrossRef] [PubMed]
2. Saliba, M.; Matsui, T.; Domanski, K.; Correa-Baena, J.-P.; Nazeeruddin, M.K.; Zakeeruddin, S.M.; Tress, W.; Abate, A.; Hagfeldt, A.; Gratzel, M. Cesium-containing triple cation perovskite solar cells: Improved stability, reproducibility and high efficiency. *Energy Environ. Sci.* **2016**, *9*, 1989–1997. [CrossRef] [PubMed]
3. Saidaminov, M.I.; Almutlaq, J.; Sarmah, S.; Dursun, I.; Zhumekenov, A.A.; Begum, R.; Pan, J.; Cho, N.; Mohammed, O.F.; Bakr, O.M. Pure Cs4PbBr6: Highly Luminescent Zero-Dimensional Perovskite Solids. *ACS Energy Lett.* **2016**, *14*, 840–845. [CrossRef]
4. Akkerman, Q.A.; Rainò, G.; Kovalenko, M.V.; Manna, L. Genesis, challenges and opportunities for colloidal lead halide perovskite nanocrystals. *Nat. Mater.* **2018**, *17*, 394–405. [CrossRef]
5. Vale, B.R.C.; Socie, E.; Burgos-Caminal, A.; Bettini, J.; Schiavon, M.A.; Moser, J.-E. Exciton, Biexciton, and Hot Exciton Dynamics in CsPbBr3 Colloidal Nanoplatelets. *J. Phys. Chem. Lett.* **2020**, *11*, 387–394. [CrossRef]
6. Cao, F.; Yu, D.; Xu, X.; Han, Z.; Zeng, H. CsPbBr3@Cs4PbBr6 Emitter-in-Host Composite: Fluorescence Origin and Interphase Energy Transfer. *J. Phys. Chem. C* **2021**, *125*, 3–19. [CrossRef]
7. Yin, J.; Maity, P.; De Bastiani, M.; Dursum, I.; Bakr, O.M.; Brédas, J.-L.; Mohammed, O.F. Molecular behavior of zero-dimensional perovskites. *Sci. Adv.* **2017**, *3*, e1701793. [CrossRef] [PubMed]
8. Akkerman, Q.A.; Park, S.; Radicchi, E.; Nunzi, F.; Mosconi, E.; De Angelis, F.; Brescia, R.; Rastogi, P.; Prato, M.; Manna, L. Nearly monodisperse insulator Cs4PbX6(X = Cl, Br, I) nanocrystals, their mixed halide compositions, and their transformation into CsPbX3 nanocrystals. *Nano Lett.* **2017**, *17*, 1924–1930. [CrossRef]
9. Cha, J.-H.; Han, J.H.; Yin, W.; Park, C.; Park, Y.; Ahn, T.K.; Cho, J.H.; Jung, D.-Y. Photoresponse of CsPbBr3 and Cs4PbBr6 Perovskite Single Crystals. *J. Phys. Chem. Lett.* **2017**, *8*, 565–570. [CrossRef]
10. Zhang, Z.; Zhu, Y.; Wang, W.; Zheng, W.; Lin, R.; Huang, F. Growth, characterization and optoelectronic applications of pure-phase large-area CsPb2Br5 flake single crystals. *J. Mater. Chem. C* **2018**, *6*, 446–451. [CrossRef]
11. Acharyya, P.; Pal, P.; Samanta, P.K.; Sarkar, A.; Pati, S.K.; Biswas, K. Single pot synthesis of indirect band gap 2D CsPb2Br5 nanosheets from direct band gap 3D CsPbBr3 nanocrystals and the origin of their luminescence properties. *Nanoscale* **2019**, *11*, 4001–4007. [CrossRef]
12. Protesescu, L.; Yakunin, S.; Bodnarchuk, M.I.; Krieg, F.; Caputo, R.; Hendon, C.H.; Yang, R.X.; Walsh, A.; Kovalenko, M.V. Nanocrystals of cesium lead halide perovskites (CsPbX3, X = Cl, Br, and I): Novel optoelectronic materials showing bright emission with wide color gamut. *Nano Lett.* **2015**, *15*, 3692–3696. [CrossRef] [PubMed]
13. Hoffman, J.B.; Zaiats, G.; Wappes, I.; Kamat, P.V. CsPbBr3 Solar Cells: Controlled Film Growth through Layer-by-Layer Quantum Dot Deposition. *Chem. Mater.* **2017**, *29*, 9767–9774. [CrossRef]
14. Gualdrón-Reyes, A.F.; Yoon, S.J.; Barea, E.M.; Agouram, S.; Muñoz-Sanjosé, V.; Meléndez, Á.M.; Niño-Gómez, M.E.; Mora-Seró, I. Controlling the Phase Segregation in Mixed Halide Perovskites through Nanocrystal Size. *ACS Energy Lett.* **2019**, *4*, 54–62. [CrossRef]
15. Hu, Y.; Wang, Q.; Shi, Y.-L.; Li, M.; Zhang, L.; Wang, Z.-K. Vacuum-evaporated all-inorganic cesium lead bromine perovskites for high-performance light-emitting diodes. *J. Mater. Chem. C* **2017**, *5*, 8144–8149. [CrossRef]
16. Sánchez, S.; Vallés-Pelarda, M.; Alberola-Borràs, J.-A.; Vidal, R.; Jerónimo-Rendón, J.J.; Saliba, M.; Boix, P.P.; Mora-Seró, I. Flash infrared annealing as a cost-effective and low environmental impact processing method for planar perovskite solar cells. *Mater. Today* **2019**, *31*, 39–46. [CrossRef]
17. Yin, J.; Zhang, Y.; Bruno, A.; Soci, C.; Bakr, O.M.; Brédas, J.-L.; Mohammed, O.F. Intrinsic Lead Ion Emissions in ZeroDimensional Cs4PbBr6 Nanocrystals. *ACS Energy Lett.* **2017**, *2*, 2805–2811. [CrossRef]
18. Clasen, B.; Sánchez, R.; Fakharuddin, A.; Mora-Seró, I. A Comparative Study of Light-Emitting Diodes Based on All-Inorganic Perovskite Nanoparticles (CsPbBr3) Synthesized at Room Temperature and by a Hot-Injection Method. *ChemPlusChem* **2018**, *83*, 294–299. [CrossRef]
19. Zhang, Y.; Kim, S.-G.; Lee, D.-K.; Park, N.-G. CH3NH3PbI3 and HC(NH2)2PbI3 Powders Synthesized from Low-Grade PbI2: Single Precursor for High-Efficiency Perovskite Solar Cells. *ChemSusChem* **2018**, *11*, 1813–1823. [CrossRef] [PubMed]
20. Vidal, R.; Alberola-Borràs, J.-A.; Mora-Seró, I. Abiotic depletion and the potential risk to the supply of cesium. *Resour. Policy* **2020**, *68*, 101792. [CrossRef]
21. Chen, Y.; Zhang, L.; Zhang, Y.; Gao, H.; Yan, H. Large-area perovskite solar cells—A review of recent progress and issues. *RSC Adv.* **2018**, *8*, 10489–10508. [CrossRef]

22. Demazeau, G. Solvothermal reactions: An original route for the synthesis of novel materials. *J. Mater. Sci.* **2008**, *43*, 2104–2114. [CrossRef]
23. Pinto, F.M.; Dey, S.; Duarte, T.M.; Taft, C.A.; La Porta, F.A. Perovskite-like quantum dots designed for advanced optoelectronic applications. In *Functional Properties of Advanced Engineering Materials and Biomolecules*; La Porta, F., Taft, C., Eds.; Springer: Cham, Switzerland, 2021. [CrossRef]
24. Tsai, H.; Nie, W.; Blancon, J.C.; Stoumpos, C.C.; Asadpour, R.; Harutyunyan, B.; Neukirch, A.J.; Verduzco, R.; Crochet, J.J.; Tretiak, S.; et al. High-efficiency two-dimensional Ruddlesden–Popper perovskite solar cells. *Nature* **2016**, *536*, 312–316. [CrossRef]
25. Dracopoulos, V.; Kastrissios, D.T.; Papatheodorou, G.N. Raman Spectra and Structure of PbCl2−ACl (A = K, Cs) Melts. *Polyhedron* **2005**, *24*, 619–625. [CrossRef]
26. Velázquez, M.; Ferrier, A.; Péchev, S.; Gravereau, P.; Chaminade, J.-P.; Portier, X.; Moncorge, R. Growth and Characterization of Pure and Pr3+-Doped Cs4PbBr6 Crystals. *J. Cryst. Growth* **2008**, *310*, 5458–5463. [CrossRef]
27. Jung, Y.-K.; Calbo, J.; Park, J.-S.; Whalley, L.D.; Kim, S.; Walsh, A. Intrinsic doping limit and defect-assisted luminescence in Cs4PbBr6. *J. Mater. Chem. A* **2019**, *7*, 20254–20261. [CrossRef]
28. Kubelka, P.; Munk-Aussig, F. Ein Beitrag zur Optik der Farban striche. *Zeit. Tech. Phys.* **1931**, *12*, 593.
29. De Bastiani, M.; Dursun, I.; Zhang, Y.; Alshankiti, B.A.; Miao, X.-H.; Yin, J.; Yengel, E.; Alorousu, E.; Turedi, B.; Almutlaq, J.M.; et al. Inside Perovskites: Quantum Luminescence from Bulk Cs4PbBr6 Single Crystals. *Chem. Mater.* **2017**, *29*, 7108–7113. [CrossRef]
30. Shi, D.; Adinolfi, V.; Comin, R.; Yuan, M.; Alarousu, E.; Buin, A.; Chen, Y.; Hoogland, S.; Rothenberger, A.; Katsiev, K.; et al. Low trap-state density and long carrier diffusion in organolead trihalide perovskite single crystals. *Science* **2015**, *347*, 519–522. [CrossRef]
31. Song, Y.H.; Choi, S.H.; Park, W.K.; Yoo, J.S.; Kwon, S.B.; Kang, B.K.; Park, S.R.; Seo, Y.S.; Yang, W.S.; Yoon, D.H. Innovatively Continuous Mass Production Couette-taylor Flow: Pure Inorganic Green-Emitting Cs4PbBr6 Perovskite Microcrystal for display technology. *Sci. Rep.* **2018**, *8*, 2009. [CrossRef] [PubMed]
32. Longo, E.; La Porta, F.A. *Recent Advances in Complex Functional Materials: From Design to Application*; Springer: Cham, Switzerland, 2017; pp. 1–454.
33. La Porta, F.A.; Taft, C.A. *Emerging Research in Science and Engineering Based on Advanced Experimental and Computational Strategies*; Springer: Cham, Switzerland, 2020; pp. 1–530.
34. De Jesus, J.P.A.; Santos, A.C.L.; Pinto, F.M.; Taft, C.A.; La Porta, F.A. Review: Theoretical and experimental investigation of the intrinsic properties of Zn2GeO4 nanocrystals. *J. Mater. Sci.* **2021**, *56*, 4552–4568. [CrossRef]
35. Mei, J.; Wang, F.; Wang, Y.; Tian, C.; Liu, H.; Zhao, D. Energy transfer assisted solvent effects on CsPbBr 3 quantum dots. *J. Mater. Chem. C* **2017**, *5*, 11076–11082. [CrossRef]
36. Palazon, F.; Urso, C.; De Trizio, L.; Akkerman, Q.; Marras, S.; Locardi, F.; Nelli, I.; Ferretti, M.; Prato, M.; Manna, L. Postsynthesis Transformation of Insulating Cs4PbBr6 Nanocrystals into BrightPerovskite CsPbBr3 through Physical and Chemical Extraction of CsBr. *ACS Energy Lett.* **2017**, *2*, 2445–2448. [CrossRef] [PubMed]
37. Quan, L.N.; Quintero-Bermudez, R.; Voznyy, O.; Walters, G.; Jain, A.; Fan, J.Z.; Zheng, X.; Yang, Z.; Sargent, E.H. Highly Emissive Green Perovskite Nanocrystals in a Solid State CrystallineMatrix. *Adv. Mater.* **2017**, *29*, 1605945. [CrossRef] [PubMed]
38. Ling, Y.; Tan, L.; Wang, X.; Zhou, Y.; Xin, Y.; Ma, B.; Hanson, K.; Gao, H. Composite Perovskitesof Cesium Lead Bromide for Optimized Photoluminescence. *J. Phys. Chem. Lett.* **2017**, *8*, 3266–3271. [CrossRef] [PubMed]
39. Fan, H.J.; Gösele, U.; Zacharias, M. Formation of nanotubes and hollow nanoparticles based on Kirkendall and diffusion processes: A review. *Small* **2007**, *3*, 1660–1671. [CrossRef] [PubMed]
40. Udayabhaskararao, T.; Houben, L.; Cohen, H.; Menahem, M.; Pinkas, I.; Avram, L.; Wolf, T.; Teitelboim, A.; Leskes, M.; Yaffe, O.; et al. A mechanistic study of phase transformation in perovskite nanocrystals driven by ligand passivation. *Chem. Mater.* **2018**, *30*, 84–93. [CrossRef]